tvst

Article

Human Foveal Cone and Müller Cells Examined by Adaptive Optics Optical Coherence Tomography

Shin Kadomoto[1], Yuki Muraoka[1], Akihito Uji[1], Sotaro Ooto[1], Kentaro Kawai[1], Masaharu Ishikura[1], Naomi Nishigori[1], Tadamichi Akagi[1], and Akitaka Tsujikawa[1]

[1] Department of Ophthalmology and Visual Sciences, Kyoto University Graduate School of Medicine, Kyoto, Japan

Correspondence: Yuki Muraoka, 54 Shougoin Kawahara-cho, Sakyo-ku, Kyoto 606-8507, Japan.
e-mail: muraoka@kuhp.kyoto-u.ac.jp

Received: May 14, 2021
Accepted: September 1, 2021
Published: September 24, 2021

Keywords: adaptive optics; optical coherence tomography; cone cell; Müller cell; foveal cell morphology

Citation: Kadomoto S, Muraoka Y, Uji A, Ooto S, Kawai K, Ishikura M, Nishigori N, Akagi T, Tsujikawa A. Human foveal cone and müller cells examined by adaptive optics optical coherence tomography. Transl Vis Sci Technol. 2021;10(11):17, https://doi.org/10.1167/tvst.10.11.17

Purpose: The purpose of this study was to image and investigate the foveal microstructure of human cone and Müller cells using adaptive optics-optical coherence tomography.

Methods: Six healthy subjects underwent the prototype adaptive optics-optical coherence tomography imaging, which allowed an axial resolution of 3.4 µm and a transverse resolution of approximately 3 µm. The morphological features of the individual retinal cells observed in the foveola were qualitatively and quantitatively evaluated.

Results: In the six healthy subjects, the image B-scans showed hyper-reflective dots that were densely packed in the outer nuclear layer. The mean number, diameter, and density of hyper-reflective dots in the foveola were 250.8 ± 59.6, 12.7 ± 59.6 µm, and 6966 ± 1833/mm^2, respectively. These qualitative and quantitative findings regarding the hyper-reflective dots were markedly consistent with the morphological features of the foveal cone cell nuclei. Additionally, the images showed the funnel-shaped hyporeflective bodies running vertically and obliquely between the inner and external limiting membranes, illustrating the cell morphology of the foveal Müller cells.

Conclusions: Using adaptive optics, we succeeded in visualizing cross-sectional images of the individual cone and Müller cells of the human retina in vivo.

Translational Relevance: Adaptive optics-optical coherence tomography would help to improve our understanding of the pathogenesis of macular diseases.

Introduction

The human retina contains three main types of neuronal cells: photoreceptor, bipolar, and ganglion cells. These convert light into visual signals transmitted to the brain.[1] In the retinas of primates, including humans, the photoreceptors are classified into cones and rods, and the cones are densely packed in the fovea, also known as a rod-free zone. The cones permit perception at a higher spatial resolution than the rods and respond differently to the different wavelengths of light; thus, they are responsible for color vision.[2] In contrast, Müller cells are the principal retinal macroglial cells in primates, including humans.[3,4] The nucleus of a Müller cell is located in the inner nuclear layer of the retina, whereas the cell bodies extend from the inner limiting membrane (ILM) to the external limiting membrane (ELM), which were described by Heinrich Müller as "radial fibers."[5] The major role of Müller cells is thus regarded as providing anatomic, metabolic, and functional support to the retinal neurons.[4]

Optical coherence tomography (OCT) is an essential imaging device that can provide cross-sectional images of the human eye in vivo. Its noninvasiveness and high axial resolution enable depicting the nucleus of photoreceptor cells as an outer nuclear layer (ONL), and the structure of the outer aspects of the photoreceptors as an ellipsoid zone band.[6] However, in conventional spectral domain (SD)-OCT, the aberration of the ocular surface is not efficiently corrected, and the transverse resolution is currently no more than 15 µm,[7,8] which makes it extremely difficult to resolve individual cone and Müller cell bodies having a lateral width of approximately 10 µm.[9,10]

Adaptive optics (AOs) is an approach that was originally developed for correcting atmospheric fluctuation, which can obscure astronomic observations.[11] AO systems with ophthalmic imaging modalities have been able to achieve a transverse resolution of approximately 3 µm by correcting the aberration existing at the ocular surface,[12] thereby providing enface images of the retinal microstructures.[13–16] More recently, the AO system has been incorporated into OCT, and the AO-OCT approach has made it possible to obtain cross-sectional images of the retina at a microscopic level.[9,17–20] Moreover, the characteristics of individual cone mosaics of human eyes were previously examined by two-dimensional images of phase-sensitive AO-OCT.[21,22] However, the cross-sectional OCT images of the nuclei of cone cells and Müller cell bodies have not been extensively studied by AO-OCT.

Thus, the purpose of this study was to investigate whether the ultrastructures of foveal cone and Müller cells could be individually depicted with our prototype AO-OCT in vivo and clarify their morphological features in the human retina if such a depiction was possible.

Methods

This observational study was approved by the Institutional Review Board of Kyoto University Graduate School of Medicine (Kyoto, Japan) and adhered to the tenets of the Declaration of Helsinki. It was performed at the Department of Ophthalmology of Kyoto University Hospital between June 2019 and September 2020. Written informed consent was obtained from each subject before any study procedures or examinations were performed. To clarify the characteristic features of foveal cone and Müller cells on the AO-OCT images, six healthy volunteers (4 men and 2 women; aged 32, 36, 40, 60, 61, and 61 years) were enrolled in this study. To minimize the effect of the refractive error, individuals with severe myopia and hyperopia were excluded.

Evaluation of the Fovea With Conventional SD-OCT

We examined the OCT images of the right eye of each subject. Each studied eye was fully dilated before imaging by administering one dose of tropicamide (0.5%) and phenylephrine hydrochloride (0.5%) drops. Each subject was instructed to direct their gaze toward an internal fixation target and was then examined for approximately 10 min in a seated posture.

We first obtained a vertical B-scan of the fovea by using a conventional SD-OCT (Spectralis HRA + OCT, Heidelberg Engineering, Heidelberg, Germany) for each eye in the high-resolution mode. A total of 100 B-scans were averaged. The A-scan rate was 40 kHz, which was translated to a B-scan (comprising 1536 A-scans) rate of 25 Hz. The scan width was 30 degrees. The axial and transverse optical resolutions of the SD-OCT were 7 µm and 14 µm, respectively. The OCT image was exported with a size of 1536 × 496 pixels. The axial and transverse pixel resolutions were 3.5 µm/pixel and 6 µm/pixel, respectively.

AO-OCT Imaging

We developed a prototype AO-OCT system (Canon, Inc., Tokyo, Japan) that was capable of the real-time correction of ocular aberrations during imaging, with a high wavefront correction efficiency using a deformable mirror (Fig. 1).

The AO-OCT system used a superluminescent diode having a center wavelength of 855 ± 50 nm and bandwidth of 100 nm, and it achieved an axial resolution of 3.4 µm at the retina. The beam diameter was 6.7 mm at the pupil of the eye, thus producing a diffraction-limited transverse resolution of approximately 3 µm, and the depth of field was approximately 44 µm within the retina. The imaging light was set to 270 µW by calculating the incident power of the light source in accordance with the safety limits set by the American National Standards Institute (Lasers ANSftSUo; American National Standard for the Safe Use of Lasers, ANSI Z136.1-2007. American National Standards Institute; 2007).

The AO-OCT system was operated with an A-scan rate of 24 kHz, which was translated to a B-scan (comprising 448 A-scans) rate of 45 Hz. A total of 100 B-scans were acquired in 2.2 seconds. The scan width was 2.5 degrees. To improve the signal-to-noise ratio, we averaged 100 consecutive AO-OCT B-scans. The recorded AO-OCT B scan lines were stabilized to correct for eye motion by using custom software (Canon, Inc., Tokyo, Japan). The eye motion in Z (depth) direction was corrected, and a rigid registration was performed by translating and rotating the second and subsequent B-scan images, which were registered to the first reference B-scan image.

Using the AO-OCT system, we obtained vertical B-scan images centered on the foveola, strictly focusing from the vitreoretinal interface to the top and bottom of the photoreceptor layers. The field of view at the fovea was 2.5 degrees (approximately 728 µm). The AO-OCT image was exported at a size of 448 × 896

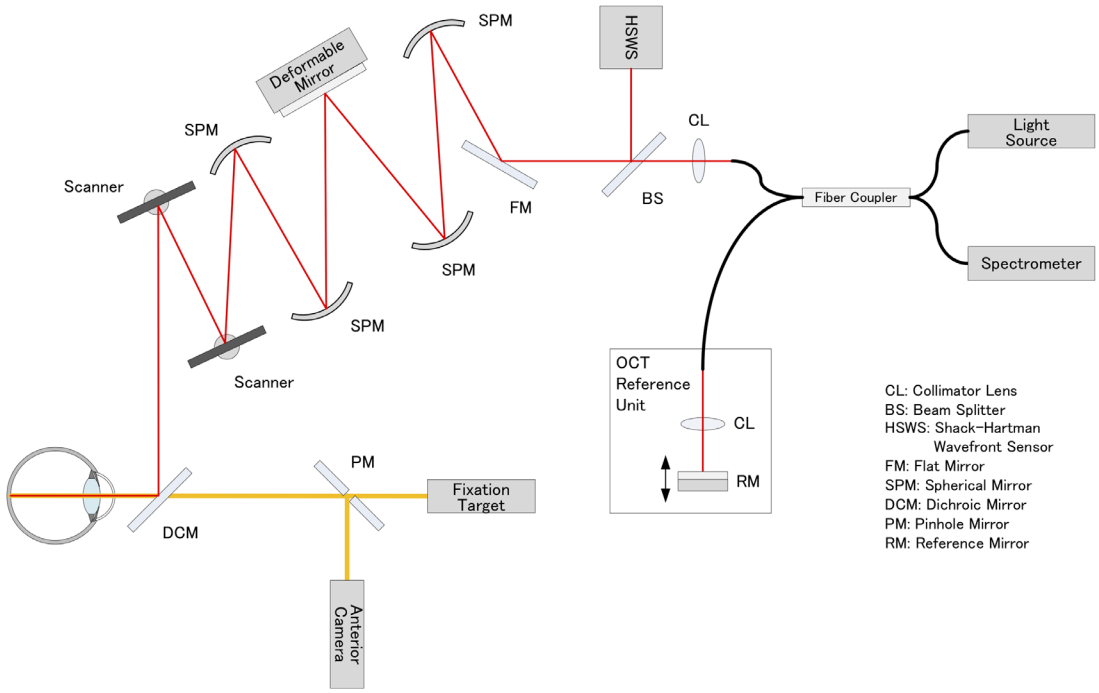

Figure 1. Schematic representation of the optical structure of adaptive optics-optical coherence tomography. Collimated near-infrared light from a superluminescent diode light source propagates through the spherical mirrors, beam splitters, and dichroic mirror to the subject's eye. Two scanners are used to scan the imaging light two-dimensionally on the retina. A 97-actuator deformable mirror is used to compensate for the eye's aberration, which is measured using a Shack–Hartman wavefront sensor. The returning light from the retina is combined with the reference light, which is reflected by the reference mirror and detected by the spectrometer.

pixels. The axial and transverse pixel resolutions were 1.16 µm/pixel and 1.63 µm/pixel, respectively.

Quantitative Evaluations of Morphology of Foveola Hyper-Reflective Dots

The foveola is the center of the fovea, and it is histologically approximately 350 to 400 µm in diameter.[10,23] The foveola lacks retinal vessels, and the retinal parenchyma only consists of the cone and Müller cells. In this study, we obtained AO-OCT images that vertically sectioned the foveola. The ONL area in the foveola was defined as the area bound by the ILM and ELM at the center 400 µm on the vertical AO-OCT image.

On the AO-OCT sections in the foveola, we detected dense hyper-reflective dots that were packed in the ONL. We measured the number and diameter of the hyper-reflective dots. First, to detect the points of the hyper-reflective dots efficiently, a Gaussian filter was applied to all the images. The software plugin, Find Maxima... (https://imagej.net/Find_Maxima...), which can determine the local maxima in images and segment particles in a binarized image per maximum, was used to detect hyper-reflective dots and to create binarized images (Figs. 2B, 2C). After the segmentation of the

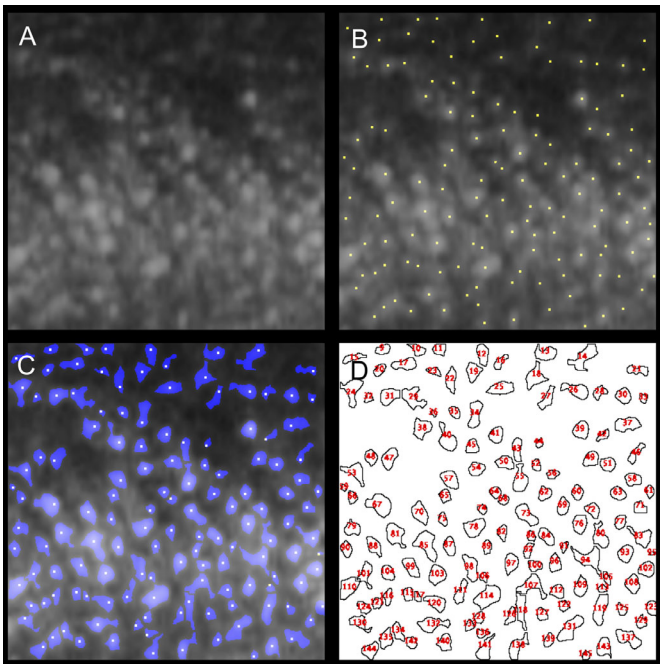

Figure 2. Representative pre- and postprocessed images illustrating the automated quantitative analysis algorithm of hyper-reflective dots. (**A**) Original image of adaptive optics–optical coherence tomography visualizing hyper-reflective dots. (**B**) Detecting hyper-reflective dots. (**C**) Segmentation of each hyper-reflective dot. (**D**) Counting and measuring the segmented area.

hyper-reflective dots within the ONL in the foveola, the mean diameter of each hyper-reflective dot was measured using the software plugin Particle Analysis (https://imagej.net/Particle_Analysis; Fig. 2D). All the processes were executed automatically using a macro that automated a series of ImageJ version 1.52b (National Institutes of Health, Bethesda, MD; https://imagej.nih.gov/ij/index.html) commands. We also measured the density of the hyper-reflective dots observed in the ONL by dividing the number of hyper-reflective dots by the area of the ONL in the foveola 400 µm.

Statistical Analyses

We performed statistical analyses using JMP 14 (SAS Institute Inc., Cary, NC, USA). The Mann-Whitney *U* test was used to compare the results between the two groups. We considered *P* values less than 0.05 to be statistically significant.

Results

We obtained high-quality AO-OCT images from all six subjects. In the healthy eyes of six subjects, we observed hyper-reflective dots that were densely packed in the ONL in the foveola, and these could not be visualized using conventional SD-OCT (Figs. 3, 4). The Table shows the quantitative measurements of the hyper-reflective dots in the healthy subjects. The ELM was depicted as a highly reflective line having a set of small pores at regular intervals of approximately 3 µm, which were not delineated with the conventional SD-OCT (see Figs. 3D, 3E).

In addition to the hyper-reflective dots, the AO-OCT delineated funnel-shaped hyporeflective bodies running vertically and obliquely between the ILM and ELM in the healthy subjects (see Fig. 4B, marked by an asterisk), suitably representing the morphologies of foveal Müller cells.

Discussion

In the current study, we succeeded in obtaining cross-sectional images of individual cone and Müller cells in the human retina in vivo by using an AO approach to OCT imaging.

AO systems equipped with a scanning light ophthalmoscope can provide enface images of retinal microstructures. Most recently, the AO system has been incorporated into OCT. However, cross-sectional OCT images of the cone and Müller cell bodies have not been fully analyzed, even by using the AO approach. The reason for this is not clearly understood; however, we speculate that it may be related to the difficulty for examiners to precisely focus on the microstructures of these cells. In this study, considering the arrangement of the cellular components from the inner to outer retinal layers of the neuroglial cells, we succeeded in imaging the individual cone and Müller cells in the

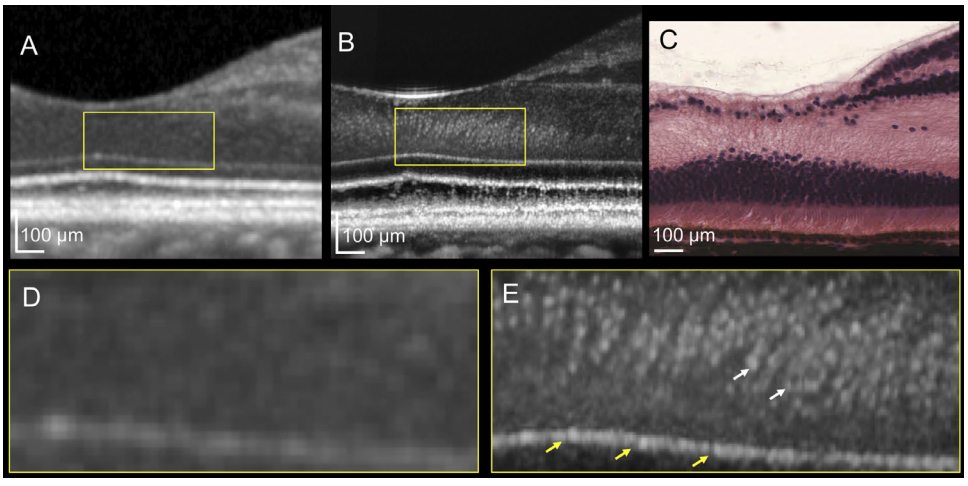

Figure 3. Photoreceptor images of the human retina depicted by optical coherence tomography (OCT). (A) Conventional spectral domain (SD)-OCT image of the fovea. (**B**) Adaptive optics (AO)-OCT image of the fovea, and (**C**) hematoxylin-eosin staining of the human fovea. (**D, E**) Magnified images of panels **A** and **B**, respectively. The AO-OCT system visualizes numerous hyper-reflective dots (*white arrow*) densely packed in the outer nuclear layer (**B**, *square*) and pores in the external limiting membrane (**B**, *yellow arrow*), neither of which are delineated with SD-OCT **A**. SD-OCT and AO-OCT images were obtained from a 32-year-old woman. Histological image courtesy of Michael Hortsch, PhD, professor of Cell and Developmental Biology and of Learning Health Sciences, University of Michigan, Medical School.

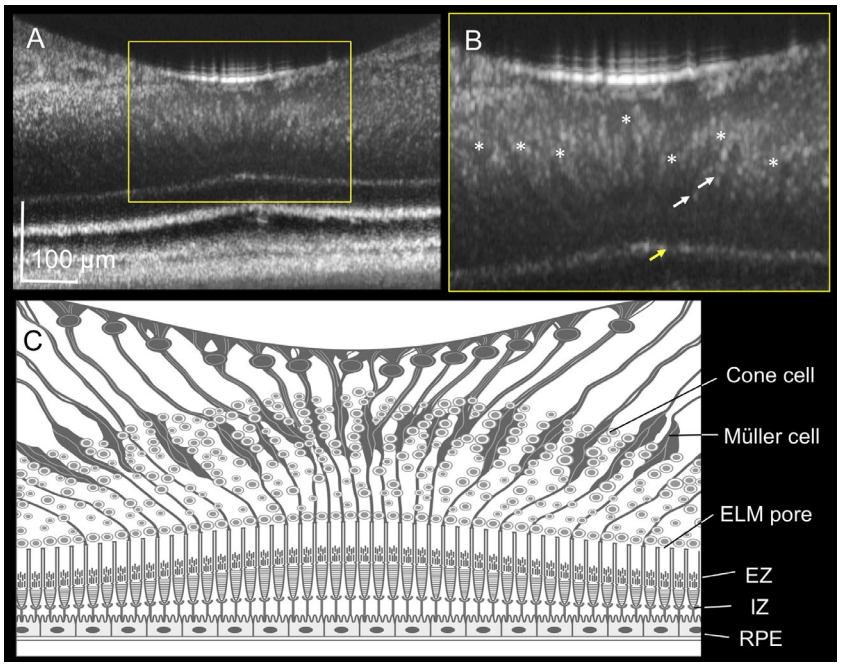

Figure 4. Foveal Müller cells elucidated by adaptive optics (AO)-optical coherence tomography (OCT). (**A, B**) The AO-OCT image and magnified image of the human fovea **B** obtained from a 60-year-old man. The AO-OCT system delineates funnel-shaped bodies running diagonally from the inner limiting membrane to the external limiting membrane (ELM; *asterisk*). (**C**) Illustration of the AO–OCT image of the fovea. The illustration shows the characteristic features of the foveal Müller cells in addition to the hyper-reflective dots in the outer nuclear layer **B** (*white arrow*) and pores in the ELM **B** (*yellow arrow*). ELM, external limiting membrane; EZ, ellipsoid zone; IZ, interdigitation zone; RPE, retinal pigment epithelium.

Table. Morphological Evaluation of the Hyper-Reflective Dots in the Foveola Using Adaptive Optics-Optical Coherence Tomography

	Total Subjects ($n = 6$)
Age (y)	48.7 ± 14.1
Refractive error (diopter)	0.53 ± 0.78
Mean axial length (mm)	23.7 ± 1.1
Central foveal thickness (μm)	204.3 ± 8.7
Area of outer nuclear layer (μm^2)	36234 ± 1833
Number of hyper-reflective dots	250.8 ± 59.6
Diameter of hyper-reflective dots (μm)	12.7 ± 4.2
Density of hyper-reflective dots (n/mm^2)	6966 ± 1833

fovea by strictly limiting the focus of the AO-OCT to the foveola. Our study showed that hyper-reflective dots in the ONL were well visualized by using AO-OCT, whereas they were not detected by conventional SD-OCT. In the AO-OCT used in this study, the focus range in the Z-axis direction was 44 μm, which is considerably narrower than the approximately 350 μm of the SD-OCT.[24] Hence, it is assumed that the AO-OCT can more easily focus on the imaging target tightly, and that the brightness and contrast in the AO-OCT images can be often superior to those in the SD-OCT images.[9] Additionally, the high transverse resolution of 3 μm in the AO-OCT may contribute to the enhancement of the image contrast. Contrarily, the transverse resolution in the SD-OCT is 15 μm. Therefore, we speculate that both the shallow depth of field and high transverse resolution in AO-OCT have a favorable effect on enhancing the image contrast.

In several AOSLO studies on cone mosaic in healthy human eyes, the density of the foveal cone mosaic was approximately 20,000 to 300,000 cones/mm^2,[16,25,26] whereas the density of the cone mosaic in human histology was 199,000 cones/mm^2;[27] both values were markedly larger than the density of hyper-reflective

dots in this study. It should be noted that the "cone mosaic" in previous reports represents the junction of the inner and outer segments (IS/OS) or ellipsoid zone of the photoreceptors. In contrast, the highly reflective dots depicted by AO-OCT in this study represent the nuclei of cone photoreceptors. In another perspective, researchers quantified the cone mosaic density in the adaptive optics scanning light ophthalmoscopy (AOSLO) images parallel to the retinal plane (sometimes referred to as C-scan). In contrast, we quantified the density of cone cell nuclei in the AO-OCT images perpendicular to the retinal plane (referred to as B-scan). The discrepancies between the results of previous reports and those of our current study are attributable to the differences in the observation targets and dimension imaged between the imaging modalities. Previous histological examination of the human retina has shown that approximately 230 cone cells are accumulated in a convex arrangement in the foveola.[1] The current study using AO-OCT also showed that the overall appearance of the hyper-reflective dots represented a convex shape, and the mean number of hyper-reflective dots was 251, which was highly consistent with the results of previous histological studies.[1,28] Because the mean diameter of the hyper-reflective dots was 12.7 μm, the hyper-reflective dots on the AO-OCT images appeared to be slightly larger than the size of the nuclei of the cone cells in the histological sections, which was reported to be 5 to 7 μm.[10] However, the human fovea is known to shrink by approximately 29% in histological sections of the retina because of tissue processing.[29] If we multiply the mean diameter of the hyper-reflective dots by 0.7, we get a value of 8.9 μm, which is close to the value of the size of cone nuclei in the retinal histology.[10] Considering the crucial difference in the methodology between AO-OCT and histology, it remains unclear whether the hyper-reflective dots in the ONL are the nuclei of cones or the nuclei and round parts of the cell bodies. However, we speculate that the hyper-reflective dots are most likely nuclei of cone cells rather than cone cell bodies.

Under a light microscope, the ELM appears as an extremely thin and fenestrated membrane.[10] Arey et al. showed that the ELM was not merely a membrane, but it was composed of a terminal bar or desmosome connecting the rod and cone cells to the terminal end of the Müller cells.[30] To date, several electron microscopic studies have supported the findings of Arey et al.[31,32] In a study using primate eyes, Cohen et al. correctly interpreted the ELM as zonulae adherens joining the inner segments of the rod and cone cells to the Müller cells.[31,32] Fenestration is observed in the inner segments of the rod and cone cells in the ELM.[33] In the present study, the AO-OCT system detected the fenestrated structure in the ELM, which was not clearly delineated on the conventional SD-OCT images. The ELM is considered a part of the retinal barrier,[33,34] and the discontinuity of the ELM may be important for the development of intraretinal and subretinal fluid in chorioretinal vascular diseases.[34–36] Therefore, observing the ELM at a high resolution may be useful for elucidating the mechanisms underlying the exudative changes.

It is markedly challenging to detect Müller cells in healthy eyes using conventional SD-OCT, although structures suggestive of Müller cells may be detected in pathological conditions.[37–39] In the current study, the AO-OCT system detected funnel-shaped bodies in the foveola running vertically and obliquely from the ILM to ELM lines, even in healthy eyes (see Fig. 4B, asterisk). Histologically, the ONL in the foveola consists of cone and Müller cells only.[3,28] We therefore believe that the funnel-shaped structure depicted the morphology of an individual Müller cell.[3,10] Müller cells are considered important macroglial cells for stabilizing the foveal structure.[40] Moreover, Müller cells are also thought to be involved in the exchange of substances with retinal neuronal cells, and the vascular permeability and absorption of exudates through communication with retinal vascular cells.[41,42] Visualization of Müller cells, which is not possible using conventional SD-OCT imaging, is expected to be useful for investigating unknown pathologies and physiology of the retina.

Our study has several limitations that should be considered when interpreting its findings. First, the sample size was very small. Second, no subjects over 70 years of age were included in this study, because the AO correction of ocular aberrations is considered a challenge for such subjects. As subjects get older, it is inevitable to obtain lens and/or vitreous opacities, and poor eye fixation. In such cases, it is difficult to adequately resolve cones or Müller cells owing to insufficient AO correction, even if they are healthy. Moreover, backscattered lights from lens and/or vitreous opacities might degrade the image quality. Therefore, the number of hyper-reflective dots in aged subjects (over 50 years old) in this study might have been underestimated because they are susceptible to signal degradation caused by media opacities. However, the quality of images for the relatively aged subjects of this study was considered adequate to visualize each hyper-reflective dot in the ONL. Third, neither horizontal AO-OCT sections nor en face evaluation from volume rendering were available because of the specifications of our current AO-OCT system. Therefore, it may not be feasible to evaluate

the three-dimensional structure of hyper-reflective dots and Müller cells in detail based on the findings of this study.

However, by using AO-OCT, we were able to visualize foveal photoreceptors and Müller cells in vivo, which had been impossible using conventional OCT imaging. This will be of considerable significance for elucidating the unknown pathophysiology of the macula that these cells may be involved in, developing new treatment protocols, and determining the efficacy of such treatments. Moreover, as the nuclei of cone cells contain genomic information, imaging of nuclei of photoreceptors would help develop novel gene therapies targeting genetic abnormalities.[43] It would also help to evaluate the severity of macular degenerative diseases, such as age-related macular degeneration, retinitis pigmentosa, and Stargardt disease, and parts of pathologies involving photoreceptor atrophy. However, if visual acuity is severely deteriorated in diseased eyes, image registration, which is essential for enhancing the image quality, can be substantially difficult and less reproducible because of the possible poor eye fixation. Therefore, the robustness of eye tracking by an AO-OCT device should be considered in cases of diseased eyes.

In conclusion, we succeeded in visualizing cross-sectional images of the individual cone and Müller cells of the human retina in vivo by using AO-OCT, which is expected to help improve our understanding of the pathogenesis of macular diseases.

Acknowledgments

Supported in part by the Japan Society for the Promotion of Science (JSPS), Tokyo, Japan (Grant-in-Aid for Scientific Research, no. 20K09771). No additional external funding was received for this study. The funders had no role in study design, data collection and analysis, decision to publish, or preparation of the manuscript.

Disclosure: **S. Kadomoto**, Nidek (R), Canon (R); **Y. Muraoka**, Bayer (R), Novartis Pharma K.K. (R), Senju (R), Nidek (R); **A. Uji**, Alcon (R), Senju (R), Canon (R); **S. Ooto**, Novartis Pharma K.K. (R), Bayer (R), Santen (R) Senju (R); **K. Kawai**, None; **M. Ishikura**, None; **N. Nishigori**, None; **T. Akagi**, Alcon (R), Kowa (R), Pfizer (R), Santen (R), Senju (R), Canon (R); **A. Tsujikawa**, Pfizer (F, R), Novartis Pharma K.K. (F, R), Bayer (F, R), Alcon (F, R), Santen (F, R), Senju (F, R), Nidek (R), Kowa (F, R), Hoya (F, R), AMO Japan (F, R)

References

1. Polyak S. The retina: The anatomy and the histology of the retina in man, ape, and monkey, including the consideration of visual functions, the history of physiological optics, and the histological laboratory technique. *JAMA*. 1942;118(15):1337.
2. Mustafi D, Engel AH, Palczewski K. Structure of cone photoreceptors. *Prog Retin Eye Res*. 2009;28:289–302.
3. Syrbe S, Kuhrt H, Gartner U, et al. Muller glial cells of the primate foveola: An electron microscopical study. *Exp Eye Res*. 2018;167:110–117.
4. Reichenbach A, Bringmann A. Glia of the human retina. *Glia*. 2020;68:768–796.
5. Müller H. Zur histologie der netzhaut. *Z Wiss Zool*. 1851;3:234–237.
6. van Velthoven ME, Faber DJ, Verbraak FD, van Leeuwen TG, de Smet MD. Recent developments in optical coherence tomography for imaging the retina. *Prog Retin Eye Res*. 2007;26:57–77.
7. Drexler W, Morgner U, Ghanta RK, Kartner FX, Schuman JS, Fujimoto JG. Ultrahigh-resolution ophthalmic optical coherence tomography. *Nat Med*. 2001;7:502–507.
8. Sánchez Brea L, Andrade De Jesus D, Shirazi MF, Pircher M, van Walsum T, Klein S. Review on retrospective procedures to correct retinal motion artefacts in OCT imaging. *Applied Sciences*. 2019;9:2700.
9. Jonnal RS, Kocaoglu OP, Zawadzki RJ, Liu Z, Miller DT, Werner JS. A Review of Adaptive Optics Optical Coherence Tomography: Technical Advances, Scientific Applications, and the Future. *Invest Ophthalmol Vis Sci*. 2016;57:OCT51–OCT68.
10. Hogan M, Alvarado J, Weddell J. *Histology of the Human Eye.: An Atlas and Textbook*. Philadelphia, PA: B, Saunders Co.; 1971;515–519.
11. Beckers JM. Adaptive optics for astronomy: principles, performance, and applications. *Ann Rev Astronomy Astrophys*. 1993;31:13–62.
12. Roorda A. Adaptive optics ophthalmoscopy. *J Refract Surg*. 2000;16:S602–S607.
13. Arichika S, Uji A, Ooto S, Muraoka Y, Yoshimura N. Effects of age and blood pressure on the retinal arterial wall, analyzed using adaptive optics scanning laser ophthalmoscopy. *Sci Rep*. 2015;5:12283.
14. Kadomoto S, Muraoka Y, Uji A, et al. Ultrastructure and hemodynamics of microaneurysms in retinal vein occlusion examined by an offset pinhole adaptive optics scanning light ophthalmoscope. *Biomed Opt Express*. 2020;11:6078–6092.

15. Roorda A, Williams DR. The arrangement of the three cone classes in the living human eye. *Nature*. 1999;397:520–522.
16. Kadomoto S, Uji A, Arichika S, et al. Macular Cone Abnormalities in Behçet's Disease Detected by Adaptive Optics Scanning Light Ophthalmoscope. *Ophthal Surg, Lasers Imag Retina*. 2021;52:218–225.
17. Karst SG, Salas M, Hafner J, et al. Three-Dimensional Analysis of Retinal Microaneurysms with Adaptive Optics Optical Coherence Tomography. *Retina*. 2019;39:465–472.
18. Hammer DX, Agrawal A, Villanueva R, Saeedi O, Liu Z. Label-free adaptive optics imaging of human retinal macrophage distribution and dynamics. *Proc Natl Acad Sci USA*. 2020;117:30661–30669.
19. Dong ZM, Wollstein G, Wang B, Schuman JS. Adaptive optics optical coherence tomography in glaucoma. *Prog Retin Eye Res*. 2017;57:76–88.
20. Shirazi MF, Brunner E, Laslandes M, Pollreisz A, Hitzenberger CK, Pircher M. Visualizing human photoreceptor and retinal pigment epithelium cell mosaics in a single volume scan over an extended field of view with adaptive optics optical coherence tomography. *Biomed Opt Express*. 2020;11:4520–4535.
21. Zhang F, Kurokawa K, Lassoued A, Crowell JA, Miller DT. Cone photoreceptor classification in the living human eye from photostimulation-induced phase dynamics. *Proc Natl Acad Sci USA*. 2019;116:7951–7956.
22. Zhang F, Kurokawa K, Bernucci MT, et al. Revealing How Color Vision Phenotype and Genotype Manifest in Individual Cone Cells. *Invest Ophthalmol Vis Sci*. 2021;62:8.
23. Cuenca N, Ortuno-Lizaran I, Sanchez-Saez X, et al. Interpretation of OCT and OCTA images from a histological approach: Clinical and experimental implications. *Prog Retin Eye Res*. 2020;77:100828.
24. Bille JF, ed. High resolution imaging in microscopy and ophthalmology: new frontiers in biomedical optics. Cham (CH): Springer; 2019.
25. Burns SA, Elsner AE, Sapoznik KA, Warner RL, Gast TJ. Adaptive optics imaging of the human retina. *Prog Retin Eye Res*. 2019;68:1–30.
26. Zhang T, Godara P, Blanco ER, et al. Variability in Human Cone Topography Assessed by Adaptive Optics Scanning Laser Ophthalmoscopy. *Am J Ophthalmol*. 2015;160:290–300.e291.
27. Curcio CA, Sloan KR, Kalina RE, Hendrickson AE. Human photoreceptor topography. *J Compar Neurol*. 1990;292:497–523.
28. Yamada E. Some structural features of the fovea centralis in the human retina. *Arch Ophthalmol*. 1969;82:151–159.
29. Curcio CA, Messinger JD, Sloan KR, Mitra A, McGwin G, Spaide RF. Human chorioretinal layer thicknesses measured in macula-wide, high-resolution histologic sections. *Invest Ophthalmol Vis Sci*. 2011;52:3943–3954.
30. Arey LB. Retina, chorioid and sclera. *Cowdry's Special Cytology*, New York, NY: Hoeber; 1932;1213.
31. Fine BS, Zimmerman LE. Observations on the rod and cone layer of the human retina: a light and electron microscopic study. *Invest Ophthalmol Vis Sci*. 1963;2:446–459.
32. Cohen AI. New details of the ultrastructure of the outer segments and ciliary connectives of the rods of human and macaque retinas. *Anatomic Record*. 1965;152:63–79.
33. Omri S, Omri B, Savoldelli M, et al. The outer limiting membrane (OLM) revisited: clinical implications. *Clin Ophthalmol*. 2010;4:183–195.
34. Daruich A, Matet A, Moulin A, et al. Mechanisms of macular edema: Beyond the surface. *Prog Retin Eye Res*. 2018;63:20–68.
35. Marmor MF. Mechanisms of fluid accumulation in retinal edema. *Doc Ophthalmol*. 1999;97:239–249.
36. Uji A, Murakami T, Nishijima K, et al. Association between hyperreflective foci in the outer retina, status of photoreceptor layer, and visual acuity in diabetic macular edema. *Am J Ophthalmol*. 2012;153:710–717.e711.
37. Ishibashi T, Iwama Y, Nakashima H, Ikeda T, Emi K. Foveal Crack Sign: An OCT Sign Preceding Macular Hole After Vitrectomy for Rhegmatogenous Retinal Detachment. *Am J Ophthalmol*. 2020;218:192–198.
38. Scharf JM, Hilely A, Preti RC, et al. Hyperreflective Stress Lines and Macular Holes. *Invest Ophthalmol Vis Sci*. 2020;61:50.
39. Govetto A, Hubschman JP, Sarraf D, et al. The role of Muller cells in tractional macular disorders: an optical coherence tomography study and physical model of mechanical force transmission. *Br J Ophthalmol*. 2020;104:466–472.
40. Gass JD. Muller cell cone, an overlooked part of the anatomy of the fovea centralis: hypotheses concerning its role in the pathogenesis of macular hole and foveomacualr retinoschisis. *Arch Ophthalmol*. 1999;117:821–823.
41. Pannicke T, Iandiev I, Wurm A, et al. Diabetes alters osmotic swelling characteristics and

membrane conductance of glial cells in rat retina. *Diabetes*. 2006;55:633–639.

42. Bringmann A, Pannicke T, Grosche J, et al. Muller cells in the healthy and diseased retina. *Prog Retin Eye Res*. 2006;25:397–424.

43. Korecki AJ, Cueva-Vargas JL, Fornes O, et al. Human MiniPromoters for ocular-rAAV expression in ON bipolar, cone, corneal, endothelial, Muller glial, and PAX6 cells. *Gene Ther*. 2021;28:351–372.

translational vision science & technology